3-D hybrid kinetic modeling of the interaction between the solar wind and lunar-like exospheric pickup ions in case of oblique/quasi-parallel/parallel upstream magnetic field

A.S. Lipatov[1,*]

GPHI UMBC/NASA GSFC, Code 673, Greenbelt, MD 20771, USA
and Faculty of Problems of Physics and Power Engineering,
Moscow Institute of Physics and Technology, Russia

W.M. Farrell, J.F. Cooper, E.C. Sittler Jr., R.E. Hartle[2]

NASA Goddard Space Flight Center, Greenbelt, MD 20771, USA

Abstract

The interactions between the solar wind and Moon-sized objects are determined by a set of the solar wind parameters and plasma environment of the space objects. The orientation of upstream magnetic field is one of the key factors which determines the formation and structure of bow shock wave/Mach cone or Alfvén wing near the obstacle. The study of effects of the direction of the upstream magnetic field on lunar-like plasma environment is the main subject of our investigation in this paper. Photoionization, electron-impact ionization and charge exchange are included in our hybrid model. The computational model includes the self-consistent dynamics of the light (H^+, He^+) and heavy (Na^+) pickup ions. The lunar interior is considered as a weakly conducting body. Our previous 2013 lunar work, as reported in this journal, found formation of a triple structure of the Mach cone near the Moon in the case of perpendicular upstream magnetic field. Further advances in modeling now reveal the presence of strong wave activity in the upstream solar wind and plasma wake in the cases of quasi-parallel and parallel upstream magnetic fields. However, little wave activity is found for the opposite case with a perpendicular upstream magnetic field. The modeling does not show a formation of the Mach cone in the case of $\theta_{B,U} \approx 0°$.

*Tel.: +1 3012860906, Fax: +1 3012861648
Email addresses: Alexander.Lipatov-1@nasa.gov (A.S. Lipatov), William.M.Farrell@nasa.gov, John.F.Cooper@nasa.gov, Edward.C.Sittler@nasa.gov, Richard.E.Hartle@nasa.gov (W.M. Farrell, J.F. Cooper, E.C. Sittler Jr., R.E. Hartle)
URL: home page (A.S. Lipatov)

[1]

[2]Additional information about the second and third authors

Keywords: Exospheres; pickup ions; induced magnetospheres; Mach cone; plasma wake; satellites
PACS: 96, 96.25.Jz, 96.25.Qr, 96.25.St, 96.30.Nd

1. Introduction

The solar wind plasma, lunar surface regolith, and neutral exosphere are all intimately interconnected in complicated ways. For example, solar energy can release neutrals from the surface, but these neutrals can become ionized and provide photoions that feed back and affect the incoming solar wind. In this paper, we continue to examine this newly appreciated environmental system feedback pathway. Earlier observations, as reviewed in Lipatov et al. (2013b), showed the existence of neutrals such as He, Na, K, and O. Detected ion species included $H^+, He^{++}, He^+, C^+, O^+, Na^+, K^+$, and Ar^+. The experiments on board of the Lunar Atmosphere and Dust Environment Explorer (LADEE) also provide new information about He, Ar, Ne, potassium, sodium, OH, H2O, Si, Al, Mg, Ca, Ti, and Fe neutral components (see e.g. Benna et al. (2014), Colaprete et al. (2014)).

There is a long history of plasma simulations of the lunar environment, as also reviewed in Lipatov et al. (2013b), the next step in our work being to include photoion pickup and reflected ions and consider how these substantial populations affect the solar wind flow. While magnetohydrodynamic (MHD) models have been useful for a study of the global configuration of the plasma structures near the Moon, important kinetic effects have not been included in the MHD formalism: namely, anisotropy of the ion velocity distribution resulting in excitation of the low-frequency electromagnetic waves, formation of the electron and ion beams and excitation of the high-frequency waves, etc. These effects may be recovered by using hybrid or full kinetic modeling. These models take into account finite ion gyroradius effects and provide an understanding not only on the solar wind flow past the object, but also of the solar wind- pickup ion interaction.

We apply various orientations of the incoming magnetic field ($\theta_{B,U} = 60°$; 45°; 0°) to a model of the neutral exosphere with H, He, Na species. We use a code which combines a Boltzmann's "particle-in-cell" approach (Lipatov et al., 1998), together with a hybrid plasma model (Lipatov et al., 2002b) in three spatial dimensions (see, e.g. Lipatov and Combi (2006)). Charge exchange between upstream and pickup ions and the exospheric neutrals is also included.

2. Hybrid model description

A quasi-neutral hybrid model is used for a kinetic description of the upstream and implanted pickup ions, and a fluid description of electrons, to study the interaction between the solar wind and the ionized and neutral components of the lunar environment (Lipatov, 2002; Lipatov et al., 2013b). This model describes well the wave-particle interactions on the ion spatial and time scales

($\rho_{\rm ci} = U_0/\Omega_{\rm i}$ and $\omega \leq \Omega_{\rm i}$), where $\rho_{\rm ci}$ is the gyroradius for ions. U_0 and $\Omega_{\rm i}$ denote the upstream velocity and the ion gyrofrequency. Our model takes into account ionization and charge exchange. The finite conductivity of the Moon's interior is also included.

Figure 1 presents an illustration of the interaction between the solar wind and the Moon. In our modeling coordinate system, the X axis is directed away from the Sun, Y axis is oriented in the direction of Earth's orbital plane and Z axis completes the right-handed system. Note that the position of the center of the Moon is $x = 0, y = 0, z = 0$.

Mass and charge state of the ions under consideration are M_s and $Z_s = 1$, where the ion population subscript s is $s = 1$ for H^+ upstream ions and $s = 2, 3, 4$ for H^+, He^+, and Na^+ pickup ions. Charge exchange between ions and neutral particles is computed with Eqs. (12-15) from Lipatov and Combi (2006).

In the following we review for convenience the electron and electric field formulations from Lipatov et al. (2013b). The electric field is computed from a standard generalized Ohm's law (Braginskii, 1965):

$$\mathbf{E} = -\frac{\nabla p_{\rm e}}{e n_{\rm e}} + \frac{\mathbf{J}_{\rm e} \times \mathbf{B}}{e n_{\rm e} c}. \tag{1}$$

The right-hand side of this equation consists of terms with the electron pressure $p_{\rm e} = n m_{\rm e} \langle v_{\rm e}'^2 \rangle / 3 = n_{\rm e} T_{\rm e}$ and the electron current $\mathbf{J}_{\rm e}$, where $v_{\rm e}'$ denotes the electron thermal velocity.

The electron density is computed from the quasi-neutrality condition

$$n_{\rm e} = n_{\rm H^+,up} + n_{\rm H^+,PI} + n_{\rm He^+,PI} + n_{\rm Na^+,PI}. \tag{2}$$

We also apply an adiabatic process for the partial pressures of all electron populations:

$$p_{\rm e} \propto (n_{\rm i,up}^{5/3} + \sum_s \frac{\beta_{\rm e,PI,s}}{\beta_{\rm e}} n_{\rm i,PI,s}^{5/3}), \tag{3}$$

where $\beta_{\rm e}$ and $\beta_{\rm e,PI,s}$ denote electron betas for the upstream and pickup populations, respectively. We also assume here that $n_{\rm e,up} = n_{\rm i,up}$, and $n_{\rm e,PI,s} = n_{\rm i,PI,s}$. The ion kinetic approach accurately includes effects of mass loading, ion pressure anisotropy, exospheric penetration by ions, and asymmetry of lunar plasma flows.

The electron stimulated desorption (Mclain et al., 2011) and photoionization are assumed to be the main mechanisms for ion production from the neutral exosphere of the Moon.

The equation for production of new ions from a three-species neutral exosphere near the Moon is similar to our four-species exosphere model (Lipatov et al., 2013b) and corresponds to

$$P_{\rm exo,k} = \nu_{i,k} n_{\rm exo,k} \eta(\theta, \phi) \exp[(r - r_{\rm exobase})/h_{\rm exo,k}]. \tag{4}$$

Here, $n_{{\rm exo},k}$ is the maximum value of the neutral density at the exobase, where $r_{\rm exobase} \approx R_{\rm M}$ (lunar radius). Index k denotes exospheric species. The exospheric densities, spatial scales, initial thermal velocities of pickup ions and

effective ionization rates are chosen in the same manner as in Lipatov et al. (2013b). The maximum values of the neutral density at the exobase are $n_{\rm exo,H} = 1.0 \times 10^2\,{\rm cm}^{-3}$, $n_{\rm exo,He} = 2.0 \times 10^3\,{\rm cm}^{-3}$, and $n_{\rm exo,Na} = 1.0 \times 10^2\,{\rm cm}^{-3}$. Spatial scales are: $h_{\rm exo,Na} = 87\,{\rm km}$, $h_{\rm exo,H} = 1990\,{\rm km}$, $h_{\rm exo,He} = 498\,{\rm km}$ (Hartle and Killen, 2006) and $v_{th,pi} = 2.0\,{\rm km/s}$.

Effective values of the ionization per atom or molecule are: $\nu_{\rm i,H} = 7.5 \times 10^{-7}\,{\rm s}^{-1}$, $\nu_{\rm i,He} = 7.8 \times 10^{-9}\,{\rm s}^{-1}$ (Wang et al., 2011b), and $\nu_{\rm i,Na} = 1.8 \times 10^{-5}\,{\rm s}^{-1}$ (Potter and Morgan, 1988; Gruntman, 1996; Wang et al., 2011b). Total pickup ion production rates are: $G_{\rm H^+} \approx 5.0 \times 10^{21}\,s^{-1}$, $G_{\rm He^+} \approx 1.0 \times 10^{21}\,s^{-1}$, and $G_{\rm Na^+} \approx 2.0 \times 10^{22}\,s^{-1}$. These values may be converted to the following mass production rates: $m_{\rm H^+} G_{\rm H^+} \approx 8.35 \times 10^{-3}\,g/s$, $m_{\rm He^+} G_{\rm He^+} \approx 6.68 \times 10^{-3}\,g/s$, and $m_{\rm Na^+} G_{\rm Na^+} \approx 7.682 \times 10^{-1}\,g/s$. The pickup ions of variable weight are generated with algorithm described in Lipatov (2012).

At the flank boundaries a damping boundary condition for the electromagnetic field has been applied. At the downstream boundary magnetic field perturbations and particles may escape the computational domain. A portion of the particles may re-enter into the computational domain from the outflow plasma. The upstream values of the magnetic field and electric fields are the same as in the solar wind.

We assume that ion bulk velocity equals to zero inside the Moon. The finite conductivity of the lunar core is taken into account with the effective magnetic Reynolds number $R_{\rm m,core} = 4\pi U_0 L \sigma_{\rm eff,core}/c^2$.

When pickup ions pass through the surfaces $y = \pm(0.5DY - 5 \times \Delta y)$, or $z = \pm(0.5DZ - 5 \times \Delta z)$, or $x = 16L - 5 \times \Delta x$ we remove them from computational domain. The particles are absorbed when they intersect the lunar surface. We do not use any boundary condition for the electromagnetic field at the lunar surface. Inside the Moon, we use our equations for the electromagnetic field with internal conductivity and the ion bulk velocity. The variations of the value of the conductivity and ion bulk velocity across the lunar surface create a jump in the electric field.

A computational domain is chosen with following dimensions $DX = 21\,L$, $DY = 30\,L$, and $DZ = 20\,L$. Here the spatial scale L equals the lunar radius $R_{\rm M}$. The computational domain contains a grid of $211 \times 301 \times 201$ points. 10^9 macro-protons and 10^8 macro-pickup ions were used in the modeling. The numerical time step Δt is chosen to satisfy the condition $\Delta t \leq \min(\Delta x, \Delta y, \Delta z)/(16 v_{max})$, where v_{max} denotes the maximum value of the macro-particle velocity.

A homogeneous solar wind plasma flow was used to start a modeling. An external electromagnetic field has upstream value: $\mathbf{B} = \mathbf{B}_0$ and $\mathbf{E} = -\mathbf{U}_0 \times \mathbf{B}_0/c$. In the lunar interior the electric field is $\mathbf{E} = 0$ and the magnetic field is $\mathbf{B} = \mathbf{B}_0$. The ion bulk velocities also equal to zero.

For chosen values of the upstream magnetic field and the local bulk velocity the values of the gyroradius of pickup ions (He^+, Na^+) and upstream ions (H^+) are about 800 km, 4500 km and 200 km (respectively). According the analysis from Winske et al. (1985) we have good resolution for the low-frequency waves and insufficient resolution for the high-frequency waves.

3. Results

In our simulation we have adopted the following input parameters. The solar wind velocity is $U_0 = 305\,\mathrm{km/s}$, $\mathbf{U} = (1.0, 0.0, 0.0)\,U_0$; the density is $n_0 = n_{\mathrm{H}^+} = 3.0\,\mathrm{cm}^{-3}$ and the value of the magnetic field is $B_0 = 5.2\,\mathrm{nT}$. In oblique case $\mathbf{B} = (-2.6, 0.0, 4.5)\,\mathrm{nT}$; in quasi-parallel case $\mathbf{B} = (-3.69, 0.0, 3.69)\,\mathrm{nT}$ and in parallel case $\mathbf{B} = (-5.2, 0.0, 0.0)\,\mathrm{nT}$. The Alfvén and sonic Mach numbers are: $M_\mathrm{A} = 5.2$ and $M_\mathrm{S} = 3.7$. Plasma betas are: $\beta_{\mathrm{H}^+} = 0.2$, $\beta_\mathrm{e} = 0.5$ and $\beta_{\mathrm{pickup,e}} = 0.05$. Inside the undersurface shell the effective Reynolds number is $R_{\mathrm{m,shell}} = 0.05$ whereas inside the lunar conducting core is $R_{\mathrm{m,core}} = 0.2$. Here, the lunar conducting core has a radius of $R_\mathrm{M}/2$.

Our modeling has been performed up to ten average transition times for particles from the upstream boundary to the downstream boundary, $t = 10\,T_{\mathrm{transit}}$.

3.1 Solar wind-Moon interaction in case with $\theta_{U,B} = 60°$

Consider first a case for oblique upstream magnetic field. Figure 2 (top) shows the cuts of Na^+ pickup ion density. The heavy Na^+ pickup ions create an asymmetrical plasma wake due to rotation around the external magnetic field.

Figure 2 (bottom) shows the density of H^+ pickup ions. The modeling shows a formation of asymmetrical halo with light pickup ions near the Moon. The plasma wake has an orientation oblique to the incoming magnetic field. The dynamics of light pickup ions are not similar to that observed in the perpendicular interaction Lipatov et al. (2013b).

Figure 3 (top) shows the solar wind H^+ ion density. The background plasma creates an asymmetrical plasma wake due to mass loading by the heavy pickup ions creating increased ion density on the outer boundary ($y < 0$, Fig. 3, top). The central region of the plasma wake is shifted slightly in both y and z compared to the nominal solar wind flow.

At the exobase the solar wind density is $n_{\mathrm{H}^+,max} \approx 1.0\,n_0$ in the case with an oblique magnetic field. The density of various species of pickup ions is: $n_{\mathrm{H}^+} \approx 2.0 \times 10^{-4}\,n_0$, $n_{\mathrm{He}^+} \approx (1.5 - 3.0) \times 10^{-5}\,n_0$, $n_{\mathrm{Na}^+} \approx 3.0 \times 10^{-4}\,n_0$. Normalization density is $n_0 = 3\,\mathrm{cm}^{-3}$. A jump in the proton density across the Mach cone is about $0.3\,n_0$ inside the cut located at $x/L = 3.0$. At the larger distance ($x/L \geq 10$) the jump in proton density becomes weaker.

The magnetic field (B_z) profile has also an asymmetrical configuration with reduced value in upper part ($y > 0$) and increased value in lower part ($y < 0$), (Fig. 3, bottom). In the day side of the exosphere one can see a jump in the value of the magnetic field (magnetic barrier), $\Delta B_z \approx 0.2\,B_0$. A jump in the magnetic field across the Mach cone is about $0.3\,B_0$. There are no visible fluctuations in the magnetic field in upstream and plasma wake.

The feature of our modeling of the solar wind-Moon interaction in case of oblique upstream magnetic field is the formation of a strong asymmetrical Mach cone, asymmetrical heavy and light ion plasma wakes, and asymmetrical inductive magnetotail. The mass loading of exo-ions should have a real and observable effect on the wake plasma and magnetic structure. Onboard measurements of

ions and magnetic field in the lunar plasma wake will allow to make a conclusion about the composition of pickup ions and their sources. This modeling prediction makes this application unique.

3.2 Solar wind-Moon interaction in case with $\theta_{U,B} = 45°$

Consider now the case of a quasi-parallel upstream magnetic field. Figure 4 demonstrates 2-D cuts of the (H^+, Na^+) pickup ion density. The $x-y$ cuts (left column) are located at $z = 0$, $y-z$ cuts (middle column) are located at $x/L = 3.0$, and $x-z$ cuts (right column) are located at $y = 0$. Let us consider first the distribution of light pickup ions. Figure 4 (bottom) shows the cuts of the distribution of the H^+ pickup ions density. Pickup ions create an asymmetrical halo around the Moon. The plasma wake has an asymmetrical form and an oblique orientation along the incoming magnetic field. This asymmetry is created by the polarization electric field in the exosphere. A more diffusive structure compared to the oblique case may be explained by formation of the shell velocity distribution and wave activity in this case.

The Na^+ pickup ion density is shown in Figure 4 (top). The $x-y$ cuts (left column) are located at $z = 0$, $y-z$ cuts (middle column) are located at $x/L = 3.0$, and $x-z$ cuts (right column) are located at $y = 0$. The Na^+ pickup ion creates an asymmetrical wake due to gyroradius. Figure 5 (top) shows the solar wind H^+ ion density. The background plasma wake has an asymmetrical plasma wake due to mass loading by the heavy pickup ions with increased ion density on the outer boundary ($y < 0$, Fig. 5, top). The central region of the plasma wake is mildly oblique to the solar wind bulk velocity.

Figures 4 and 5 gives the following variation in the densities of background and pickup ions at the exobase in case with quasi-parallel magnetic field: $n_{H^+} \approx 1.\, n_0$, $n_{H^+} \approx 1.2 \times 10^{-4}\, n_0$, $n_{He^+} \approx (1.5 - 3.0) \times 10^{-5}\, n_0$, $n_{Na^+} \approx 2. \times 10^{-4}\, n_0$. $n_0 = 3.0\,\mathrm{cm}^{-3}$ is upstream solar wind density. A jump in the proton density across the Mach cone is about $0.15\, n_0$.

The magnetic field (B_z) has reduced value in upper part ($y > 0$) and increased value in lower part ($y < 0$), (Fig. 5, bottom). A jump in the magnetic field across the Mach cone is about $0.15\, B_0$, and it is smaller than in the case of $\theta_{B,U} = 60°$. Upstream, 1-D cuts show the following perturbations in the magnetic field with amplitude about of $\delta B_y \approx 0.01 B_0$ and $\delta B_z \approx 0.01 B_0$, and wave-length about of $\lambda \approx 1400\,\mathrm{km}$. Downstream, 1-D cuts show much stronger perturbations in the magnetic field with amplitude about of $\delta B_y \approx 0.01 B_0$ and $\delta B_z \approx 0.01 B_0$, and wave-length about of $\lambda \approx 1200\,\mathrm{km}$.

Once again, we conclude that for a quasi-parallel B-field configuration, the mass loading of the exo-ions creates a modified solar wind flow, changes the orientation of the plasma wake and alters the structure of the tailing B-field (compared to the 'unloaded' situation). Pickup ions have a clear and obvious effect on the near-Moon plasma interaction.

3.3 Solar wind-Moon interaction in case with $\theta_{U,B} \approx 0°$

Consider now the case of a parallel upstream magnetic field. Figure 6 demonstrates 2-D cuts of the (H^+, Na^+) pickup ion density. The $x-y$ cuts (left col-

umn) are located at $z = 0$, $y - z$ cuts (middle column) are located at $x/L = 3.0$, and $x - z$ cuts (right column) are located at $y = 0$. Let us consider at first the distribution of light pickup ions. Figure 6 (bottom) shows the cuts of the distribution of the H^+ pickup ions. Pickup ions create a halo around the Moon which is transformed into the relatively thin tail along the lunar plasma wake.

The Na^+ pickup ion density is shown in Figure 6 (top). The $x - y$ cuts (left column) are located at $z = 0$, $y - z$ cuts (middle column) are located at $x/L = 3.0$, and $x - z$ cuts (right column) are located at $y = 0$. The Na^+ heavy pickup ions form a halo near the Moon and a complex tail structure rotating around the magnetic field. The trajectory of the heavy Na^+ pickup ions in the outer tail is similar to a test particle motion with an average value of the gyroradius about of 3×10^4 km.

The modeling does not demonstrate a formation of the Mach cone in the solar wind H^+ ion density profile (Fig. 7, top). The central region of the plasma wake is slightly oblique to the solar wind bulk velocity.

Figure 7 (bottom) shows a distribution of the B_z magnetic field. This figure demonstrates an asymmetrical tail and strong perturbations in the magnetic field but without a formation of Mach cone. Upstream, 1-D cuts show the following perturbations in the magnetic field with amplitude about of $\delta B_y \approx 0.02 B_0$ and $\delta B_z \approx 0.02 B_0$, and wave-length about of $\lambda \approx 1500$ km. Downstream, 1-D cuts show much stronger perturbations in the magnetic field with amplitude about of $\delta B_y \approx 0.1 B_0$ and $\delta B_z \approx 0.1 B_0$, and wave-length about of $\lambda \approx 1000$ km.

The modeling gives the following range of variation in densities of the solar wind and pickup ions at the lunar exobase in the case with parallel magnetic field: $n_{H^+} = 1.\, n_0$, and $n_{H^+} \approx (1.0 - 6.0) \times 10^{-4}\, n_0$, $n_{He^+} \approx (1.0 - 3.0) \times 10^{-4}\, n_0$, $n_{Na^+} \approx 1.5 \times 10^{-3}\, n_0$. $n_0 = 3.\, \mathrm{cm}^{-3}$ denotes upstream density.

Finally, the modeling shows that the physics of mass loading is different in this parallel case. We find that the E-field is muted when $\mathbf{U}$ is parallel to $\mathbf{B}$ and that the driving $\mathbf{E} = \mathbf{U} \times \mathbf{B}$ may be reduced or even disappear in this case. The coupling between the solar wind and pickup ions is only available through the excitation of the kinetic Alfvén and compressional waves similar parallel mass loading in case of comets (see e.g. the 2.5-D modeling by Galeev et al. (1987)). The modeling in Galeev et al. (1987) shows the transformation of a ring-type velocity distribution of pickup ions with a small thermal velocity to the shell velocity distribution. The thermal velocity of pickup ion shell velocity distribution becomes comparable with a local speed of the solar wind. The pickup ions are accelerated by the electric field perturbations excited due to beam-solar wind plasma instabilities in opposite the case with an oblique upstream magnetic field. No magnetic barrier was observed in modeling.

The structures of plasma environment near the Moon observed in our modeling (asymmetrical Mach cone, plasma wake, pickup ion exospheres, asymmetrical plasma tails and excitation of the magnetic field perturbations) need to be compared with the measurements by the particles and magnetic field instruments on the ARTEMIS P1 spacecraft. This task can confirm the value of our solar wind – lunar exosphere interaction models.

4. Conclusions

The hybrid modeling of lunar plasma environment with three pickup ion species and various orientations of the upstream magnetic field has demonstrated several features:

- In the case of oblique ($\theta_{B,U} \approx 60^\circ$) and quasi-parallel ($\theta_{B,U} \approx 45^\circ$) upstream magnetic field, the magnetic barrier has the same structure as was observed in the modeling in case of quasi-perpendicular upstream magnetic field (Lipatov et al., 2013b).

- For oblique and quasi-parallel upstream magnetic field pickup ions provide drive formation of the asymmetrical Mach cone. The heavy Na^+ ions form an asymmetrical tail across the upstream magnetic field due to finite gyroradius. The light H^+ pickup ions form an asymmetrical tail oblique to the direction of upstream magnetic field.

- In the case of parallel upstream magnetic field the mechanism of the solar wind mass loading with pickup ions is mostly produced by the excitation of the Alfvén and magnetosonic waves due to beam-solar wind plasma instabilities. Pickup acceleration is determined by the electric field perturbations from these instabilities (see e.g. (Winske et al., 1985)). There is no magnetic field barrier on the sun-side lunar surface. The mass loading does not result in formation of Mach cone in case of parallel ($\theta_{B,U} \approx 0^\circ$) upstream magnetic field. The light and heavy pickup ions fill in the lunar plasma wake.

- For upstream magnetic field in the range ($0^\circ \leq \theta_{B,U} \leq 45^\circ$), pickup ions generate the electromagnetic perturbations upstream and in the lunar plasma wake.

- The results of this work may be important for understanding the plasma processes in the plasma environment near very weak comets, asteroids, Pluto, and Europa (Sauer et al., 1997; Lipatov et al., 1997, 2010a, 2013a).

Acknowledgments

This work was supported in part by a NASA Project: *Dynamic Response of the Environment at Asteroids, the Moon, and the moons of Mars* (DREAM2) (PI: W. Farrell) and a grant *Solar Wind Interaction with Lunar Exosphere and Surface* (PI - J.F. Cooper) from the NASA NRA: Lunar Advance Science and Exploration Research Program (NNH08ZDA001-LASER). A.S.L. was also supported in part by the grant/task 670-90-315 between the GPHI UMBC and NASA GSFC. Computational resources were provided by the NASA Ames Advanced Supercomputing (NAS) Division (Pleiades/Ivy-Bridge, Projects SMD-13-3913 and SMD-14-4816).

References

Benna, M., Mahaffy, P.R, & Hodges, R.R., 2014. In: Lunar Dust and Exosphere - The First Results from LADEE, 45th Lunar and Planetary Science Conference, The Woodlands, Texas, 2014.

Birch, P.C., Chapman, S.C., 2001. Detailed structure and dynamics in particle-in-cell simulations of the lunar wake. Physics of Plasmas 8, 4551-4559.

Braginskii, S.L., 1965. Transport processes in a plasma. In: Leontovich, M.A. (Ed.), *Reviews of Plasma Physics*. Consultants Bureau, (New York, pp. 205-240).

Colaprete, A., Elphic, R.C., Landis, D., Karcz, J., Shirley, M., et al., 2014. Overview of the LADEE Ultraviolet-Visible Spectrometer: Design, Operations, and Initial Results. In: Lunar Dust and Exosphere - The First Results from LADEE, 45th Lunar and Planetary Science Conference, The Woodlands, Texas, 2014.

Galeev, A.A., Lipatov, A.S., Sagdeev, R.Z., 1987. Two-dimensional numerical simulation of the relaxation of cometary ions and MHD turbulence in the flow of the solar wind around a cometary atmosphere. Sov. J. Plasma Phys. 13(5), 323.

Gruntman, M., 1996. H_2^+ pickup ions in the solar wind: Outgassing of interplanetary dust. J. Geophys. Res. 101(A7), 15555-15568.

Farrell, W.M., Kaiser, M.L., Steinberg, J.T., Bale, S.D., 1998. A simple simulation of a plasma void: Applications to Wind observations of the lunar wake. J. Geophys. Res. 103(A10), 23653-23660.

Hartle, R.E., Killen, R., 2006. Measuring pickup ions to characterize the surfaces and exospheres of planetary bodies: applications to the Moon. Geophys. Res. Lett. 33, L05201, 1-5.

Hartle, R.E., Thomas, G.E., 1974. Neutral and Ion Exosphere Models for Lunar Hydrogen and Helium. J. Geophys. Res. 79(10), 1519-1526.

Holmström, M., Fatemi, S., Futaana, Y., Nilsson, H., 2012. The interaction between the Moon and the solar wind. Earth Planets Space 64(2), 237-245.

Kallio, E., 2005. Formation of the lunar wake in quasi-neutral hybrid model, Geophys. Res. Lett. 32, L06107, 1-5.

Lipatov, A.S., 2002. *The Hybrid Multiscale Simulation Technology: an introduction with application to astrophysical and laboratory plasmas*, Springer-Verlag, (Berlin, Heidelberg, New York (pp. 1-403).

Lipatov, A.S., 2012. Merging for Particle-Mesh Complex Particle Kinetic modeling of the multiple plasma beams. J. Comput. Phys. 231, 3101-3118.

Lipatov, A.S., Combi, M.R., 2006. Effects of kinetic processes in shaping Io's global plasma environment: A 3D hybrid model. ICARUS 180(2), 412-427.

Lipatov, A.S., Cooper, J.F., Paterson, W.R., Sittler, E.C., Hartle, R.E., Simpson, D.G., 2010a. Jovian plasma torus interaction with Europa: 3-D Hybrid kinetic simulation. First results. Planet. Space Sci. 58, 1681-1691.

Lipatov, A.S., Cooper, J.F., Sittler, E.C., Hartle, R.E., 2011b. Effects of pickup ions on the solar wind near the lunar-like objects: 3-D hybrid modeling. Proceeding of the extended abstracts, European Planetary Science Congress-DPS Joint Meeting 2011, October 2-7, 2011, Nantes, France, Session TP/MG8/SB14, Vol. 6, Paper EPSC-PDS2011-95.

Lipatov, A.S., Cooper, J.F., Sittler, E.C., Hartle, R.E., 2012a. Effects of Na^+, and He^+ pickup ions on the lunar-like plasma environment: 3-D hybrid modeling. Adv. Space Res. 50, 1583-1591.

Lipatov, A.S., Cooper, J.F., Paterson, W.R., Sittler Jr., E.C., Hartle, R.E., Simpson, D.G., 2013a. Jovian plasma torus interaction with Europa. Plasma wake structure and effect of inductive magnetic field: 3-D Hybrid kinetic simulation. Planet. Space Sci. 77, 12-24.

Lipatov, A.S., Cooper, J.F., Sittler Jr., E.C., Hartle, R.E., 2013b. The light (H^+, H_2^+, He^+) and heavy (Na^+) pickup ion dynamics in the lunar-like plasma environment: 3D hybrid kinetic modeling. Adv. Space Res. 52, 1929-1938.

Lipatov, A.S., Motschmann, U., Bagdonat, T., 2002b. 3-D hybrid simulation of the interaction of the solar wind with a weak comet. Planet. Space Sci. 50, 403-411.

Lipatov, A.S., Motschmann, U., Bagdonat, T., Griessmeier, J.-M., 2005. The interaction of the stellar wind with an extrasolar planet – 3-D hybrid and drift-kinetic simulations. Planet. Space Sci. 53, 423-432.

Lipatov A.S., Sauer, K., Baumgärtel, K., 1997. 2.5-D hybrid code simulation of the solar wind interaction with weak comets and related objects. Adv. Space Res. 20(2), 279-282.

Lipatov A.S., Zank, G.P., Pauls, H.L., 1998. The interaction of neutral interstellar H with the heliosphere: A 2.5-D particle-mesh boltzmann simulation. J. Geophys. Res. 103(A9), 20631-20642.

McLain, J.L., Sprague, A.L., Grieves, G.A., Schriver, D., Travnicek, P., Orlando, T.M., 2011. Electron-stimulated desorption of silicates: A potential source for ions in Mercury's space environment. J. Geophys. Res. 116, E03007, 1-9, doi:10.1029/2010JE003714.

Potter, A.E., Morgan, T.H., 1988. Discovery of sodium and potassium vapor in the atmosphere of the Moon. Science 241, 675-680, doi:10.1126/science.241.4866.675.

Sauer, K., Lipatov, A.S., Baumgärtel, K., Dubinin E., 1997. Solar Wind-Pluto Interaction Revised. Adv. Space Res. 20(2), 295-299.

Saito, Y., Yokota1, S., Tanaka, T., Asamura1, K., Nishino, M.N., Fujimoto1, M., Tsunakawa, H., Shibuya, H., Matsushima, M., Shimizu, H., Takahashi, F., Mukai, T., & Terasawa, T., 2008. Solar wind proton reflection at the lunar surface: Low energy ion measurement by MAP-PACE onboard SELENE (KAGUYA). Geophys. Res. Lett. 35(24), L4205, doi:10.1029/2008GL036077.

Tanaka, T., Saito, Y., Yokota, S., Asamura, K., Nishino, M.N., Tsunakawa, H., Shibuya, H., Matsushima, K., Shimizu, H., Takahashi, F., Fujimoto, M., Mukai, T., 2009. First in situ observation of the Moon-originating ions in the Earth's Magnetosphere by MAP-PACE on SELENE (KAGUYA). Geophys. Res. Lett. 36, L22106, 1-5, doi:10.1029/2009GL040682.

Travnicek, P., Hellinger, P., Schriver, D., Bale, S.D., 2005. Structure of the lunar wake: Two-dimensional global hybrid simulations. Geophys. Res. Lett. 32, L06102, 1-4, doi:10.1029/2004GL022243.

Tyler, A.L., Kozlowski, R.W.H., Hunten, D.M., 1988. Observations of sodium in the tenuous lunar atmosphere. Geophys. Res. Lett. 15(10), 1141-1144, doi:10.1029/GL015i010p01141.

Wang, Y.-C., Müller, J., Ip, W.-H., Motschmann, U., 2011a. A 3-D hybrid simulation study of the electromagnetic field distributions in the lunar wake. Icarus 216, 415-425.

Wang, X.-D., Zong, Q.-G., Wang, J.-S., Cui, J. Réme, H., Dandouras, I., Aoustin, C., Tan, X., Shen, J., Ren, X., Liu, J.-J., Zuo, W., Su, Y., Wen, W.-B., Wang, F., Fu, Q., Mu, L.-L., Wang, X.-Q., Geng, L., Zhang, Z.-B., Liu, J.-Z., Zhang, H.-B., Li, C.-L., Quyang, Z.-Y., 2011b. Detection of $m/q = 2$ pickup ions in the plasma environment of the Moon: The trace of exospheric H_2^+. Geophys. Res. Lett. 38, L14204, 1-5, doi:10.1029/2011GL047488.

Wiehle, S., Plaschke, F., Motschmann, U., Glassmeier, K.-H., Auster, H.U., Angelopoulos, V., Mueller, J., Kriegel, H., Georgescu, E., Halekas, J., Sibeck, D.G., McFadden, J.P., 2011. First Lunar Wake Passage of ARTEMIS: Discrimination of Wake Effects and Solar Wind Fluctuations by 3-D Hybrid Simulations. Planet. Space Sci. 59(8), 661-671.

Winske, D., Wu, C.S., Li, Y.Y., Mou, Z.Z., Guo, S.Y., 1985. Coupling of newborn ions to the solar wind by electromagnetic instabilities and their interaction with the bow shock. J. Geophys. Res. 90, 2713-2726.

Wurz, P., Rohner, U., Whitby, J.A., Kolb, C., Lammer, H., Dobnikar, P., Martín-Fernández, J.A., 2007. The lunar exosphere: The sputtering contribution. Icarus 191, 486-496.

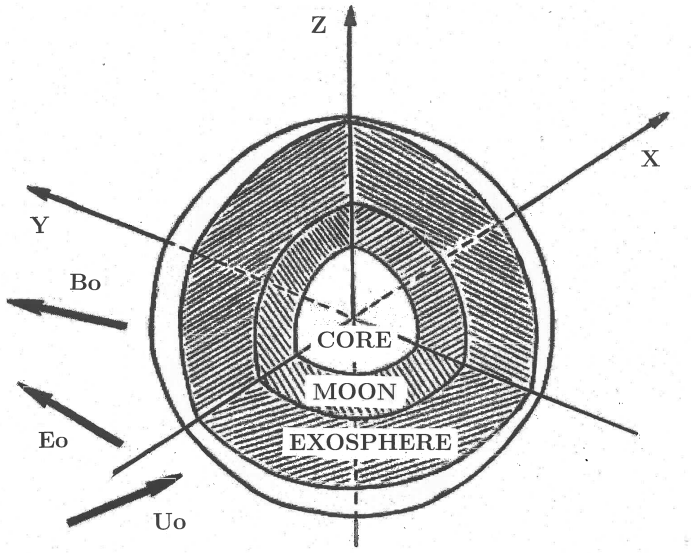

Figure 1: Lunar plasma environment and the system of coordinates.

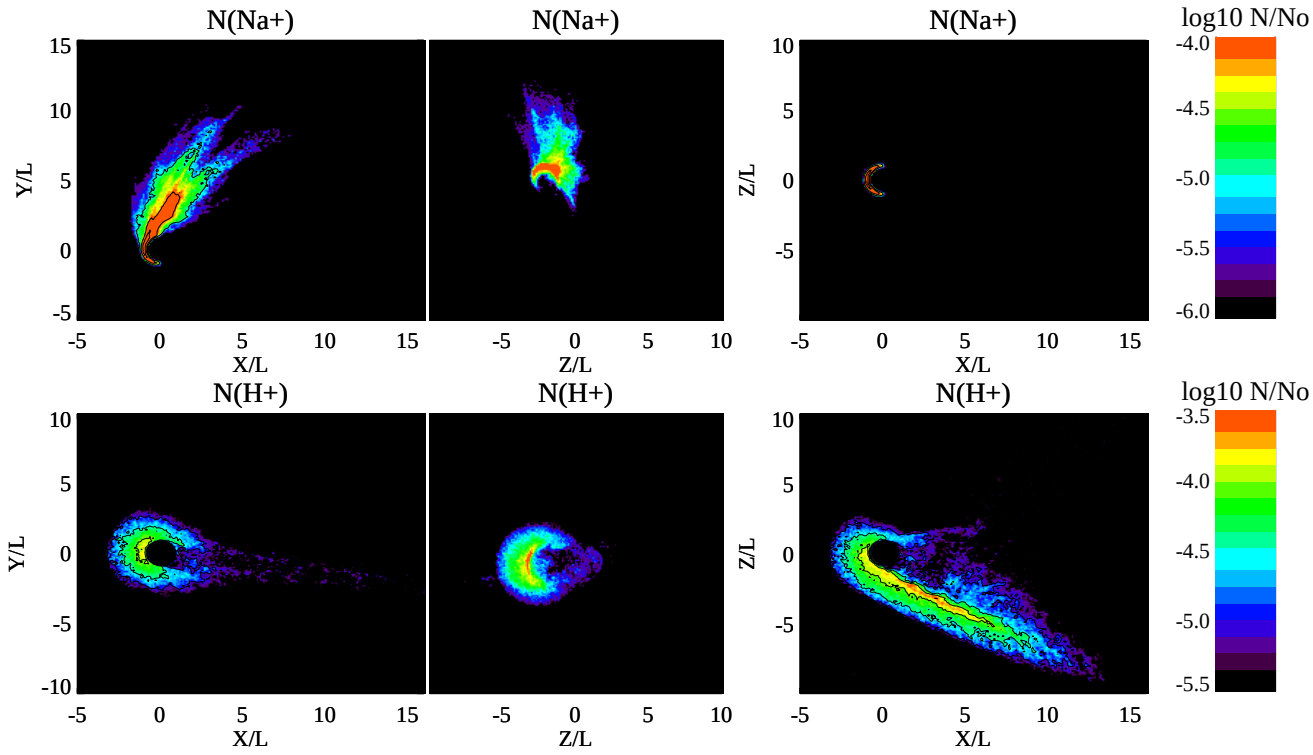

Figure 2: $\theta_{U,B} = 60°$. 2-D cuts of the Na^+, H^+ pickup ion (top and bottom) density profile. Here $N_0 = n_{H^+} = 3.0\,cm^{-3}$. x-y cuts (left column) are located at $z = 0$, y-z cuts (middle column) are located at $x/L = 3.0$, and x-z cuts (right column) are located at $y = 0$.

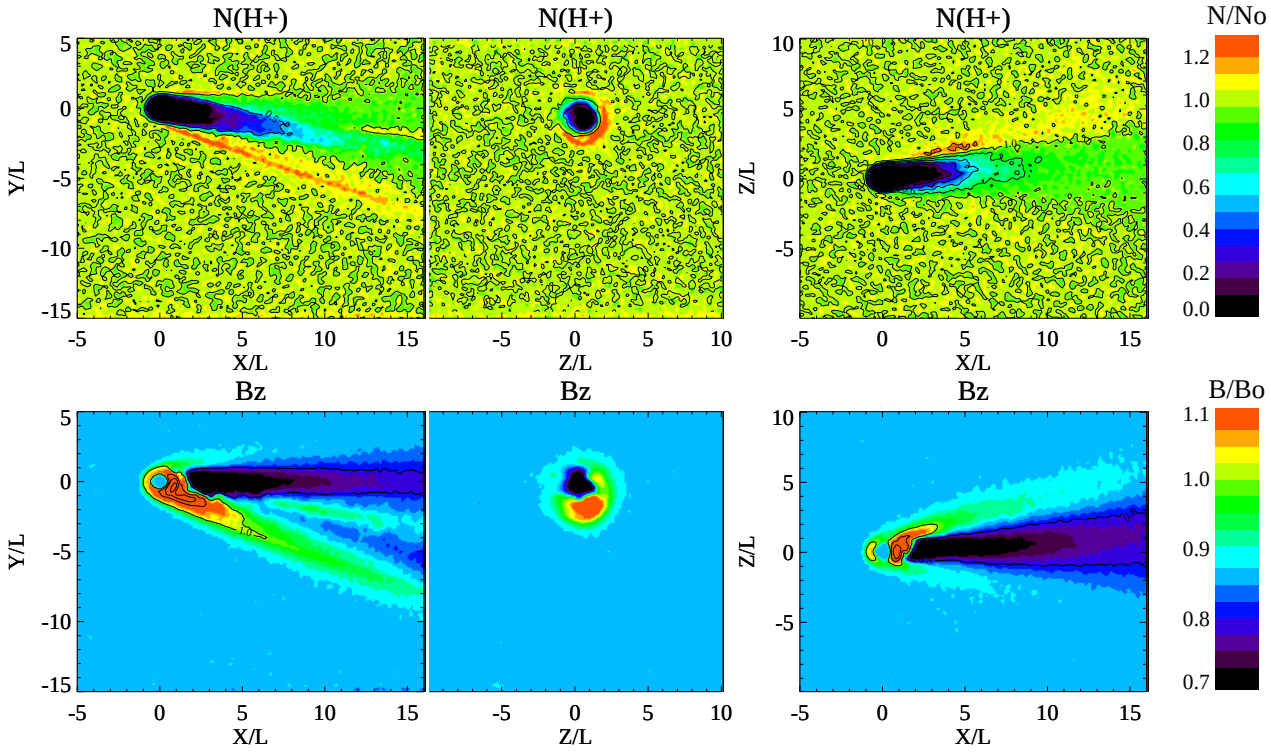

Figure 3: $\theta_{U,B} = 60°$. 2-D cuts of the upstream (background) H^+ ion density (top) and B_z magnetic field (bottom) profile. x-y cuts (left column) are located at $z = 0$, y-z cuts (middle column) are located at $x/L = 3.0$, and x-z cuts (right column) are located at $y = 0$.

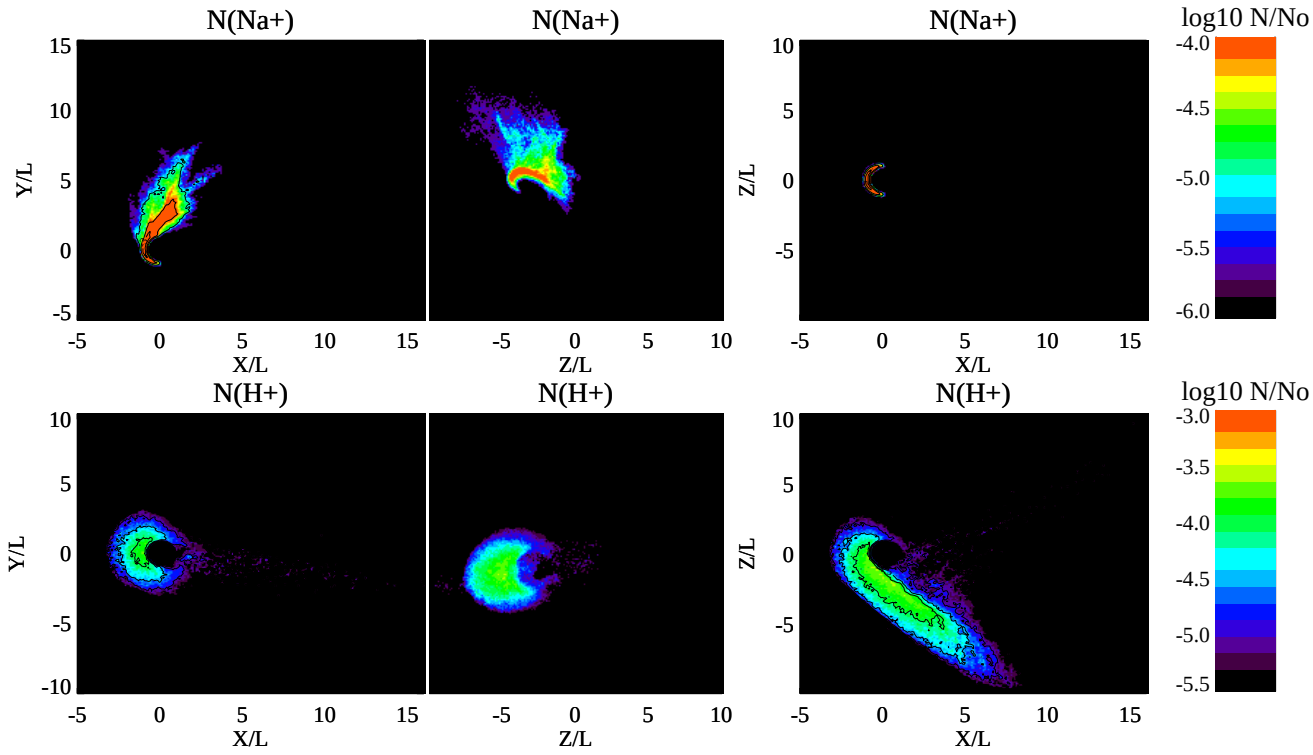

Figure 4: $\theta_{U,B} = 45°$. 2-D cuts of the Na^+, H^+ pickup ion (top and bottom) density profile. Here $N_{=}n_{H^+} = 3.0\,cm^{-3}$. x-y cuts (left column) are located at $z = 0$, y-z cuts (middle column) are located at $x/L = 3.0$, and x-z cuts (right column) are located at $y = 0$.

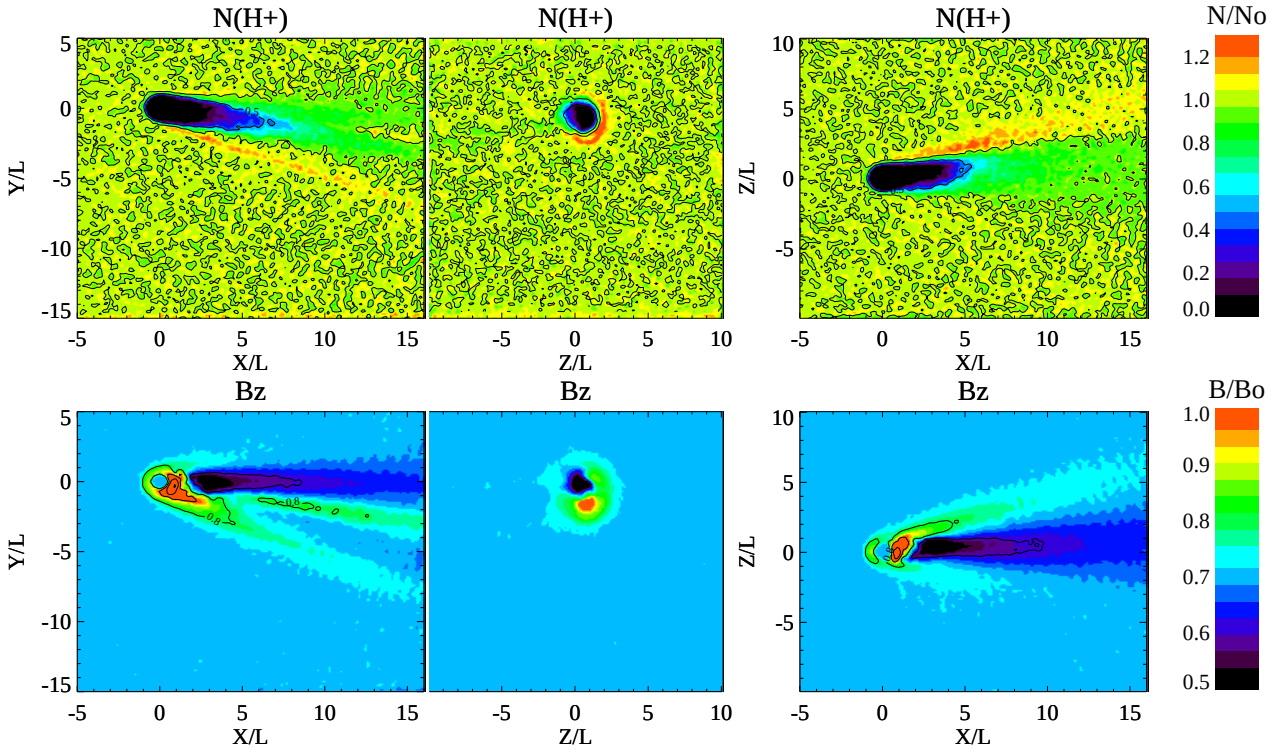

Figure 5: $\theta_{U,B} = 45°$. 2-D cuts of the upstream (background) H^+ ion density (top) and B_z magnetic field (bottom) profile. x-y cuts (left column) are located at $z = 0$, y-z cuts (middle column) are located at $x/L = 3.0$, and x-z cuts (right column) are located at $y = 0$.

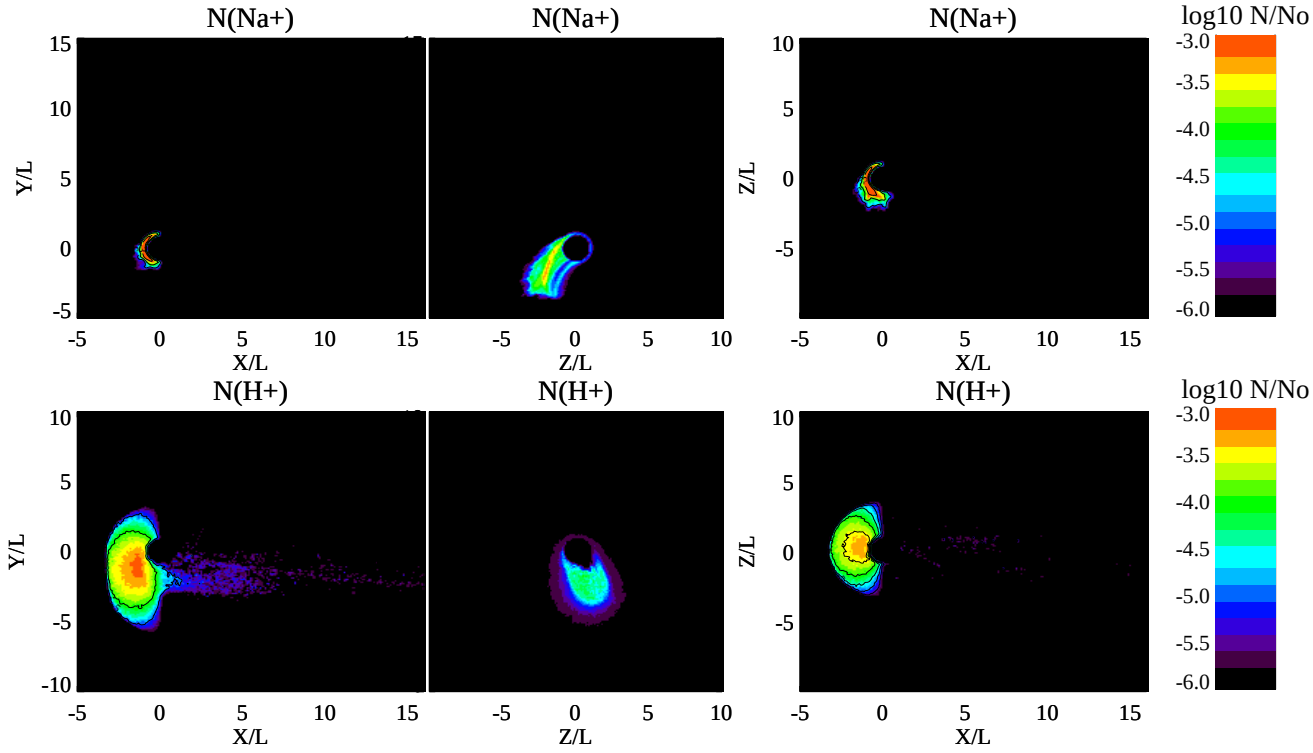

Figure 6: $\theta_{U,B} \approx 0$. 2-D cuts of the Na^+, H^+ pickup ion (top and bottom) density profile. Here $N_0 = n_{\mathrm{H}^+} = 3.0\,\mathrm{cm}^{-3}$. x-y cuts (left column) are located at $z = 0$, y-z cuts (middle column) are located at $x/L = 3.0$, and x-z cuts (right column) are located at $y = 0$.

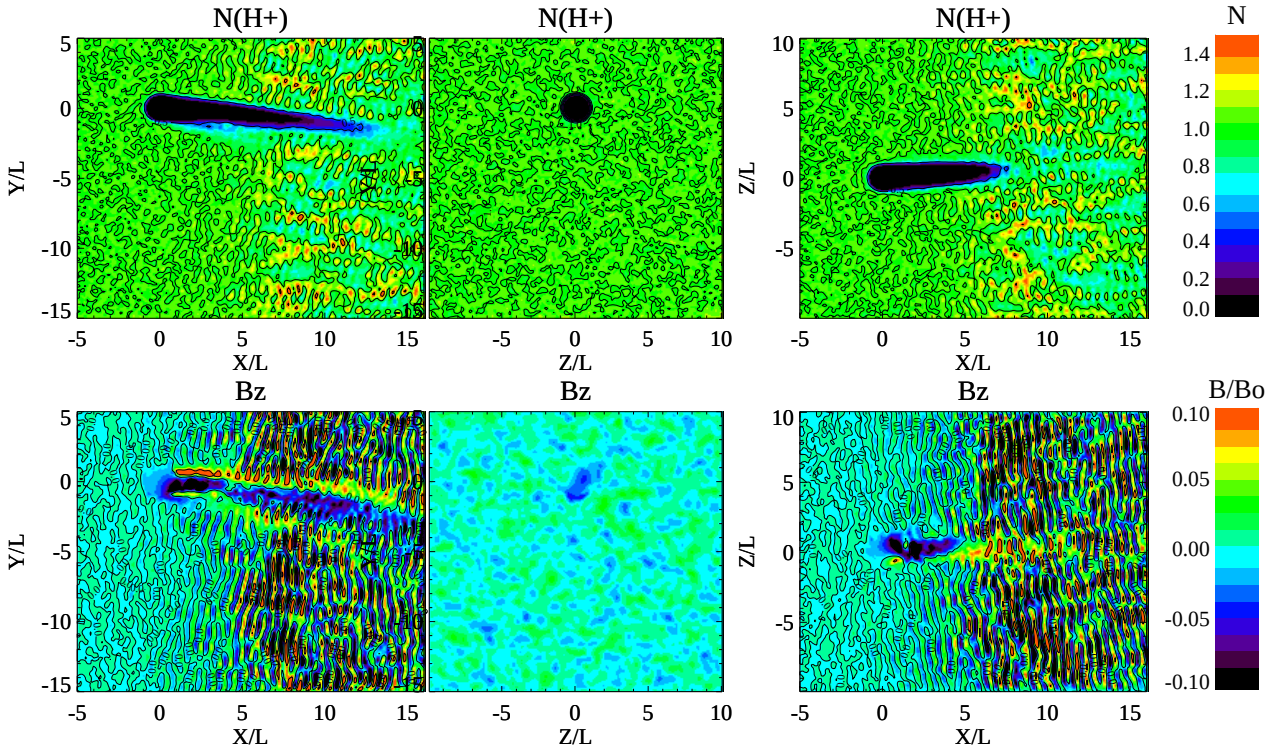

Figure 7: $\theta_{U,B} \approx 0$. 2-D cuts of the upstream (background) H^+ ion density (top) and B_z magnetic field (bottom) profile. x-y cuts (left column) are located at $z = 0$, y-z cuts (middle column) are located at $x/L = 3.0$, and x-z cuts (right column) are located at $y = 0$.